Heliyon 9 (2023) e18686

Contents lists available at ScienceDirect

Heliyon

journal homepage: www.cell.com/heliyon

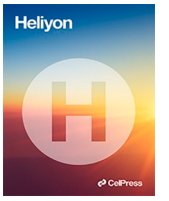

Proof of evidence of changes in global terrestrial biomes using historic and recent NDVI time series

Hadi Zare Khormizi [a], Hamid Reza Ghafarian Malamiri [b], Sahar Alian [c], Alfred Stein [d], Zahra Kalantari [e,f], Carla Sofia Santos Ferreira [f,g,h,*]

[a] *Range Management, Faculty of Natural Resources, University of Tehran, Karaj, Iran*
[b] *Remote Sensing, Department of Geography, Yazd University, Yazd, Iran*
[c] *Department of Civil Engineering, Rahman Institute of Higher Education, Ramsar, Iran*
[d] *Department of Earth Observation Science, Faculty of Geo-Information Science and Earth Observation (ITC), University of Twente, Enschede, the Netherlands*
[e] *Department of Sustainable Development, Environmental Science and Engineering, KTH Royal Institute of Technology, Stockholm, Sweden*
[f] *Department of Physical Geography and Bolin Centre for Climate Research, Stockholm University, Stockholm, Sweden*
[g] *Polytechnic Institute of Coimbra, Applied Research Institute, Coimbra, Portugal*
[h] *Research Centre for Natural Resources, Environment and Society (CERNAS), Polytechnic Institute of Coimbra, Coimbra, Portugal*

ARTICLE INFO

Keywords:
Vegetation coverage
Global biomes
Plant annual phases
Time series
Climate change

ABSTRACT

Climate change affects plant dynamics and functioning of terrestrial ecosystems. This study aims to investigate temporal changes in global vegetation coverage and biomes during the past three decades. We compared historic annual NDVI time series (1982, 1983, 1984 and 1985) with recent ones (2015, 2016, 2017 and 2018), captured from NOAA-AVHRR satellite observations. To correct the NDVI time series for missing data and outliers, we applied the Harmonic Analysis of Time Series (HANTS) algorithm. The NDVI time series were decomposed in their significant amplitude and phase given their periodic fluctuation, except for ever green vegetation. Our findings show that the average NDVI values in most biomes have increased significantly (F-value$<$0.01) by 0.05 ndvi units over during the past three decades, except in tundra, and deserts and xeric shrublands. The highest rates of change in the harmonic components were observed in the northern hemisphere, mainly above 30° latitude. Worldwide, the mean annual phase reduced by 9° corresponding to a 9 days shift in the beginning of the growing season. Annual phases in the recent time series reduced significantly as compared to the historic time series in the five major global biomes: by 14.1, 14.8, 10.6, 9.5, and 22.8 days in boreal forests/taiga; Mediterranean forests, woodlands, and scrubs; temperate conifer forests; temperate grasslands, savannas, and shrublands; and deserts, and xeric shrublands, respectively. In tropical and subtropical biomes, however, changes in the annual phase of vegetation coverage were not statistically significant. The decrease in the level of phases and acceleration of growth and changes in plant phenology indicate the increase in temperature and climate changes of the planet.

* Corresponding author. Department of Physical Geography and Bolin Centre for Climate Research, Stockholm University, Stockholm, Sweden.
E-mail address: carla.ferreira@natgeo.su.se (C.S.S. Ferreira).

https://doi.org/10.1016/j.heliyon.2023.e18686
Received 11 July 2023; Received in revised form 22 July 2023; Accepted 25 July 2023
Available online 28 July 2023

1. Introduction

With the advent of the industrial revolution and the increasing use of fossil fuels over the past two centuries, climate change has been accelerated as a result of the emission and intensification of greenhouse gases [1]. These gases increase the atmosphere temperature and cause global warming by absorbing and dispersing infrared spectra reflected from the earth's surface [1]. Plant dynamics are influenced by environmental factors such as temperature and rainfall [2,3]. Temperature is considered the leading factor [2], whereas rainfall will be influential mainly when the temperature is optimal for plant growth [4]. Evidences show that global warming has drastically affected vegetation coverage in recent decades [5–7], and caused shifts in biome types. In India, for example, climate change has led to a decrease in the area cover for tropical desert scrubs, tropical deserts, tropical wet forests, and tropical moist forests [8].

Studding the changes in vegetation coverages and the parameters affecting it, requires the preparation of maps with frequent observations. The use of ground data collection methods is very costly, time-consuming, point-to-point and in some cases impossible. With the development of satellite imageries and remote sensing techniques, environmental factors such as temperature and rainfall are increasingly being used for analyzing plant dynamics [9]. Satellite acquisition system covers the whole word with data collected at regular intervals. For instance, the relationship between climate change and remotely-sensed vegetation indices such as the Normalized Difference Vegetation Index (NDVI) has been investigated in several studies [10–14].

Vegetation is characterized by its growth cycle (e.g. seasonal for vegetables and grains, and annual for deciduous trees). The variation of NDVI over time, during different stages of growth, can be described by a combination of periodic functions [15]. Although, this variation might not always be a complete periodic signal, it has features due to the superposition of periodic functions (i.e. monthly and yearly). This indicates that time series of NDVI can be characterized by combinations of different components of a periodic function (e.g. cosine and sine with various phase and amplitude at different periods of time). The sinusoidal cycle of plant growth is consisting of different cyclic components, such as annual and seasonal, and some noise [16]. The NDVI curve shows a combination of these components, as a unique signal which convey valuable information about the different environmental forces affecting the phenological stages of plants. These significant periodic components can be used to quantify the variation of NDVI over time by fitting a Fourier series (harmonic analysis) to the original time series data. Fast Fourier Transform (FFT) algorithm can be used to decompose a time series to its constituent signals (components). However, only some components are statistically significant which correspond to having most variance of time series and random noises. Each periodic component makes a sine or cosine signal with its amplitude and phase. Summation of all these signals can create the original signal without any noise.

The analysis of time series can therefore be helpful in identifying different vegetation coverage characteristics such as growth and phenological changes. Remote sensing time series contain much information about plant dynamics and changes [17,18]. To make optimal use of these data, continuous, gap-free, and complete data over time are required. But, remotely sensed time series data captured by satellite's sensors are often contaminated by gaps (no-data) and outliers (anomalous values compared to adjacent pixels). However, continuous remote sensing data is often degraded due to e.g. atmospheric dust, aerosols, sensor malfunction and especially cloud coverage [19], which causes errors in reading the optical sensors by affecting the energy reflected from the surface [20].

Harmonic Analysis of Time Series (HANTS) has been developed for identifying and removing outliers and filling in gaps in NDVI time series, either existing ones or created by removing outliers [21]. It decomposes the periodic time series into its components or different sines and cosines with various amplitudes and phases using Fast Fourier Transform (FFT) algorithm [22]. HANTS applies irregular sampling gaps and extracts the phenological data of plants [21,23]. For instance, HANTS has been used in recent years to reconstruct the gaps caused by cloud cover in remote sensing time series [20,24–29].

Analysis of changes in plant growth stages using HANTS (by decomposition of plant growth signal into its amplitudes and phases), especially for plants with annual fluctuation cycles, can be effective in identifying changes in plant growth and phenological processes related to climatic changes [13]. Phenology deals with the study of the time of occurrence of repeatable events of plant life in relation to the living and non-living organisms [30–32], and has a strong relationship with climatic events [32–34]. It is known as a critical biological index in response to global warming [35,36] because temperature is one of the most important factors in the initiation of plant growth and phenological processes [18,37,38].

HANTS has been used for the classification of vegetation coverages [39,40], recognizing that different types of vegetation coverage and plant species have various patterns in different components of Fourier series (significant periodic components with different amplitude and phase) [22,41]. Changes in NDVI time series components created by HANTS, however, have not yet been investigated globally. Examining vegetation changes using HANTS algorithm and basic concepts of physics can have advantages. For example, this method is less affected by the transient dynamics of vegetation.

The main objective of the present study is to investigate changes in time series components of global biomes to reveal the possible impact of climate change over the last 30 years. To do so, we used HANTS algorithm in reconstructing NDVI time series and then, extract the most significant periodic components of NDVI time series signal and relate them to biomes coverage changes.

2. Materials and methods

2.1. Study area

The study focuses on the global scale terrestrial biomes. Biomes are nature's major ecological communities, classified according to the predominant vegetation, climate, and characterized by the adaptation of organisms to a particular environment [42]. Terrestrial biomes are the major global plant communities determined by rainfall and climate. In this research, we considered the terrestrial

biomes classification proposed by Ref. [43], which includes 14 distinct biomes (Fig. 1). These biomes are based on 825 terrestrial ecoregions of the globe [43]. The map of biomes is used as a basis for the assessment of changes of harmonic components of global vegetation coverage time series.

2.2. NDVI products

Four historical annual time series (1982, 1983, 1984, and 1985) and four recent annual time series (2015, 2016, 2017, and 2018) were used to investigate the changes of harmonic components of global vegetation coverage. There are two reasons to use these time series. First, mere extraction and comparison of harmonic components of just two single NDVI time series cannot indicate the real climatic change because changes may be influenced by the transient plant dynamics such as dry and wet periods. Second, it is possible to statistically compare changes in the harmonic components using one-way ANOVA, based on two sets of four annual time series. Because of the daily temporal resolution of NOAA-AVHRR NDVI images, we used 365 images per year. The FFT algorithm which the HANTS is based on it, was used to extract annual periodic harmonic components of the time series for each year.

The NDVI is a commonly used index for the assessment of plant dynamics [7]. It is calculated by the following equation [44]:

$$NDVI = \frac{NIR - RED}{NIR + RED} \tag{1}$$

where *NIR* and *RED* represent the reflectance of near-infrared and red band, respectively. The amplitude of this index ranges between −1 and +1. Negative values show water, ice and snow areas, positive values indicate vegetation coverage increasing toward 1, while values around zero show arid or unplanted areas. In our study we exclude the negative data as they provide no evidence for vegetation. But some areas where the NDVI values were negative in historic study period, may be turn to positive values in recent period (e.g. shrinking water bodies), and vice versa.

In this study, NOAA-AVHRR NDVI images were used, with *NIR* corresponding to AVHRR-band 2 and *RED* to AVHRR-band 1. We used daily NDVI data with a spatial resolution of 0.05 × 0.05° under the name AVH13C1 (NOAA CDR Program data). The algorithm for calculation of NDVI was developed by NOAA's Climate Data Record (CDR) program using equation (1) [45].

2.3. The HANTS algorithm

In this study, we used the HANTS algorithm to solve problems in the studied time series driven by the presence of outliers and gaps, and to generate different harmonic components such as amplitude and phase images in the time series. The HANTS algorithm is based on the concept of Fast Fourier Transform (FFT) [21,23,46], which is used here for modeling our time series of satellite data (see section

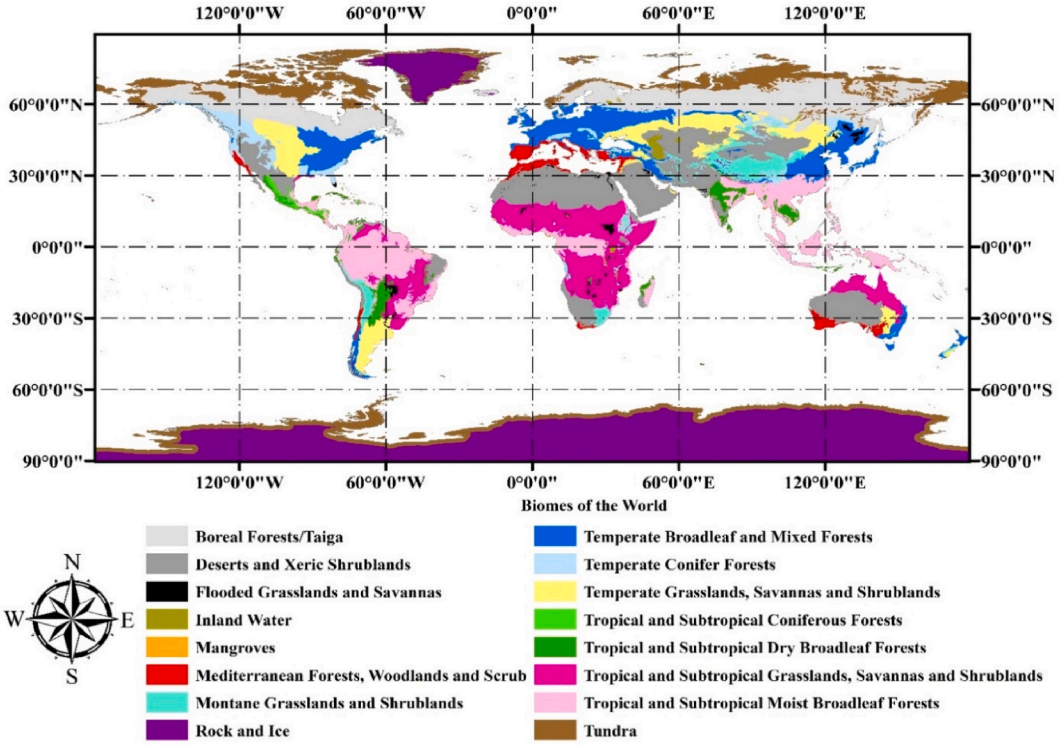

Fig. 1. Map of global biomes [43].

2.4). We briefly introduce the algorithm and explain the parameters required for obtaining a reliable model by the algorithm. Let y_i be a time series with N observations (i from 1 to N). This time series can be described by a Fourier series, as follows:

$$y_i = a_0 + \sum_{j=1}^{M} a_j \cos\left(w_j t_i - \varphi_j\right) \tag{2}$$

where w_j is the j^{th} frequency of harmonic series in a Fourier series, t_i is the time when the ith sample is taken, M is the number of frequencies of Fourier series ($M \leq N$), and aj and φj are jth amplitude and phase of the harmonic series, respectively. Since the zero frequency (a_0) has no phase, the amplitude related to a_0 is equal to the mean of all N observations y_i. The harmonic frequencies (w_j) are obtained by multiplying a base frequency (e.g. $w_j = 2\pi/N$) by I (equation (3)):

$$w_j = \left(\frac{2\pi}{N}\right) \times i \; i = 1, 2, 3, \ldots, N \tag{3}$$

In the HANTS algorithm, after selecting M and the w_j, the unknown Fourier series parameters of a_j and phase values φ_j are determined by fitting the time series through observations using the least square method. To obtain a reliable model from a time series, several parameters should be defined by the user [21].

1. A valid data range, e.g. the acceptable range of observed values. Observations outside this range stage are eliminated by allocating zero weight to them.
2. The relevant period, e.g. the number of samples in each periodic component.
3. The Number of Frequencies (NOF), which determines the details that can be used in signal reconstruction. A low NOF creates a signal with less details than a large NOF.
4. Direction of outliers, indicates whether high or low values (outliers) should be rejected during curve fitting.
5. Fit Error Tolerance (FET), which determines the absolute deviation from the current value of the curve in the chosen direction that is still acceptable. After each repetition, the observations with deviations larger than the FET are designed as outliers and are eliminated by allocating zero weight to them.
6. Degree of Over-Determinedness (DOD), e.g. the minimum number of additional data points that need to be used in curve fitting. The number of valid observations should always exceed the number of parameters needed for signal description (2 × NOF-1). On the other hand, DOD is effective only for a small FET.

2.4. Fast Fourier Transform (FFT)

Decomposition of alternating functions into their components provides a useful insight into the processes of observed signal determination and their relative weight. Fourier series analysis is used for the decomposition of a complex signal into its sines and cosine components [47]. Thus, equation (2) can be written as a matrix relation, following equations (4) and (5):

$$\begin{pmatrix} y_1 \\ \vdots \\ y_N \end{pmatrix} = \begin{pmatrix} f_1(t_1) & \cdots & f_M(t_1) \\ \vdots & \ddots & \vdots \\ f_1(t_N) & \cdots & f_M(t_N) \end{pmatrix} \begin{pmatrix} a_1 \\ \vdots \\ a_M \end{pmatrix} \tag{4}$$

$$y = Fa \tag{5}$$

By multiplying the two sides of the relation by the transpose of matrix F, we will have equation (6):

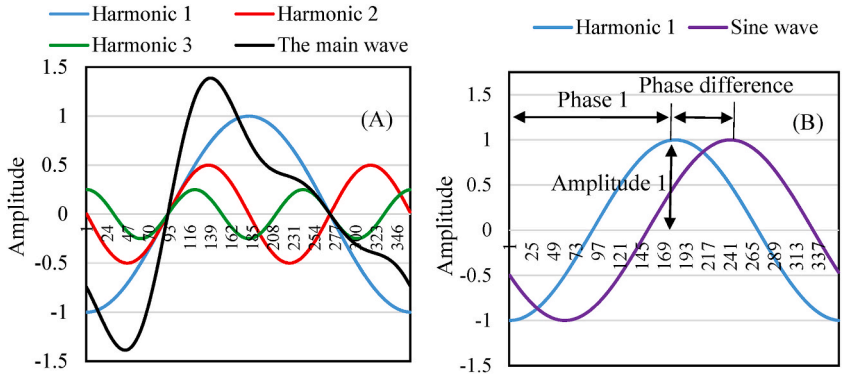

Fig. 2. Hypothetical signal (black wave) and its harmonic components (A), and amplitude, phase, and phase difference concepts (B), following Fast Fourier Transform function.

$$F^T y = F^T F a \text{ or } a = \left(F^T F\right)^{-1} F^T y \tag{6}$$

Here the vector *a* yields an estimate of amplitude and phase for each component by the least square method. The *FFT* of an algorithm is used for the calculation of matrix multiplication in equation (6) using a relatively small number of estimation operations. The results of using *FFT* in a time series with *N* data include the amplitudes and phases of all frequencies (*N* phases and *N* frequencies).

According to the Fourier series expansion, each alternating function can be obtained from the sum of several sine and cosine waves with different frequencies [47]. Hence, a non-sinusoidal wave can be disintegrated into sinusoidal components with different frequencies. If these sinusoidal waves are summed, the main waveform is obtained. For instance, we may assume that in Fig. 2A the main signal (black line) is a trend of changes for an annual NDVI. Then this wave is disintegrated in the HANTS algorithm into three cosine waves with different amplitudes and frequencies by selecting the default value of three frequencies. From the cosine waveforms, a wave with the same frequency as the main waveform is harmonic 1 and a wave with *n* frequency is harmonic *n*. Each sine or cosine wave has its own amplitude, phase, and frequency. These data are helpful in determining changes in vegetation coverage. The amplitude, phase, and phase difference concepts are shown in Fig. 2B. The wave amplitude is defined as the highest rate of transition from the mean and a phase to the fraction of the wave cycle that is elapsed relative to the origin.

2.5. Implementation of NDVI at global scale

The NDVI time series implemented for the past three decades might be different in terms of gaps and outliers. First, the percentage of invalid data (smaller than zero), in NDVI along each pixel of historical (1982, 1983, 1984, and 1985) and recent (2015, 2016, 2017, and 2018) annual time series were determined using equation (7):

$$P = \frac{K}{N} \times 100 \tag{7}$$

where P is the percentage of invalid data, including both negative NDVI values and NaN (due to clouds) at each pixel of time series, K is the number of invalid data, and N is the total number of data in the time series. After computing the percentage of invalid data in each annual time series (i.e, N = 356), the average of Ps for the four historical annual time series and for the four recent ones were calculated. Also, to visualize and compare the scatter of invalid data between both time series the average map of Ps in recent data was subtracted from the historical data.

One of the disadvantages of HANTS algorithm is no clear way to set the input parameter. To do so, we need to implement a number of pre-tests by different set of parameters on the data to reach an optimum result for gap filling. Also, based on the previous studies on reconstruction of MODIS time series done by Refs. [20,48], the input parameters in the HANTS algorithm were considered according to Table 1. Using these parameters, the outliers and gaps were reconstructed and harmonic components of time series were generated by the HANTS algorithm for each annual time series. Maps of the mean harmonic components for the four-time series in the two investigated periods were obtained, as well as their differences. A statistical comparison of the four-year means was done by using a one-way ANOVA, and maps of significant changes at 95% probability level were drawn. The studied harmonic components included amplitude 0, amplitude 1 (annual amplitude), and phase 1 (annual phase). Higher frequencies corresponding to short periods of vegetation coverage were not considered, as these are influenced by noise, gaps, and short-term changes of vegetation coverage [18, 49].

The baseline period was taken as 365 days based on the total number of images in an annual time series, and the number of frequencies (NOF) was set to 3. Dividing the baseline period by NOF, the smallest reconstruction period equals will be 122 days. Such a period is compatible with the seasonal periods of vegetation coverage changes (~four months) [20,48]. Further, the Fit Error Tolerance (FET) was set to 0.1 NDVI unit and the direction of outliers was set to 'low', given the direction of the outliers caused by cloud cover which reduces the infrared spectrum and NDVI from the actual global value. Finally, the Degree of Over-Determinedness (DOD) was set to 10.

The Root Mean Squared Error (RMSE) was used to determine the accuracy of the HANTS algorithm as well as to measure the accuracy of the curves fitted to the raw data to generate the harmonic components in the NDVI time series. It was computed using equation (8):

Table 1
Parameters used for reconstruction of NDVI images by HANTS algorithm.

Parameters	Rate
Valid data range	0–1
Baseline period	365 images
Number of Frequency (NOF)	3
Fit Error Tolerance (FET)	0.1
Direction of outliers	LOW
Degree of Over-Determinedness (DOD)	10

$$RMSE = \sqrt{\frac{\sum_{i=1}^{n}(x_i - y_i)^2}{n}} \quad (8)$$

where x_i and y_i are the actual and estimated data, respectively, and n is the total number of data.

Finally, the changes of amplitude and phase for each harmonic components of the historical and recent time series, both globally and for the individual biomes, were investigated.

3. Results

3.1. Invalid NDVI data and reconstruction of data series

The percentage of invalid data (gaps) in each pixel (Eq. (7)) during the four historic and recent annual NDVI time series are shown in Fig. 3. The mean number of invalid data (Fig. 3A–B) in the historical and recent time series on the Earth's surface are 53% and 42%, respectively, with gaps decreasing over the past three decades. Generally, the number of invalid data in the time series between 30° N and 30° S is smaller than that of around 60° N.

The harmonic components are extracted based on the curve fitted to the original data. By investigating the reconstruction error, we noted that the HANTS algorithm effectively reconstructed the gaps and outliers in the time series. For example, Fig. 4 shows the results of the curve fitted to the original data along one pixel in 1982 (Figs. 4A) and 2018 (Fig. 4B) (temporal). The spatial differences in mean RMSE between the original and the reconstructed data during the four-years historical and recent time series are shown in Figs. 5A–6B, respectively. Mean RMSE around the world range between 0.08 and 0.10 NDVI unit, except in Antarctica (south pole), Greenland, and other vegetation-free regions (e.g. deserts and xeric shrublands in Fig. 1). On the whole, the reconstruction error in most regions is between 0.06 and 0.12 NDVI unit.

3.2. Harmonic components (aplitudes and phases) of NDVI time series

In this section, to illustrate and compare the status of global vegetation coverage in the recent and historic annual NDVI time series, the mean and difference between amplitudes and phases of harmonic periodic components are presented.

At first, for example, the signal of changes in NDVI time series, and its harmonic components was studied on a selected pixel of deciduous tree areas (to see the sinusoidal variation of growing stages from spring through summer and fall to winter) in 1982 and 2018. Fig. 6 (A) illustrates the reconstruction results of an annual time series along one pixel in 1982 and 2018, and Fig. 6 (B) shows the results of decomposition of these growth curves into harmonic components in 1982 and 2018. According to Fig. 6 (B), amplitude 0 (a_0) in 2018 exceeded that in 1982, indicating a rise in the overall vegetation coverage. Furthermore, phase 1 (φ_1) (red and black continuous lines) are decreased in 2018. The decrease of phase 1 shows that the growing season and phenological processes in 2018 start earlier than in 1982 along this pixel. Moreover, harmonic amplitude 1 (a_1) is increased in the 2018 time series.

3.2.1. Spatial variation in mean NDVI between time series

The maps of mean NDVI (or amplitude 0) of four historic annual time series and four recent annual time series are shown in Fig. 7A–B, respectively. As indicated, the areas close to the North Pole, central Australia, and central North America have a low amplitude 0 (<0.15 NDVI unit). Highest amplitude 0 (0.4–0.8 NDVI unit) is found in the northern forests, located around 60° N and other regions with high vegetation coverage percentage such as evergreen broadleaf, South American forests, center of African, Eastern North American and European forests. In general, the highest value of the amplitude 0 corresponds to the tropical and subtropical moist broadleaf forests and temperate broadleaf and mixed forests biomes.

To clearly represent the changes during the past three decades, the mean harmonic 0 map of the present time was subtracted from the mean harmonic 0 map of the past time (Fig. 8). As shown in Fig. 8A, the areas close to the North Pole and some other regions like

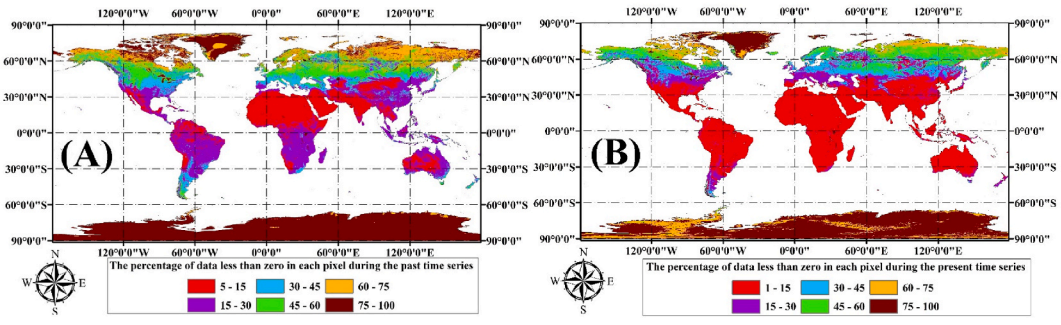

Fig. 3. Percentage of mean invalid data (NDVI<0) in four historic (1982, 1983, 1984, and 1985) (A) and four recent (2015, 2016, 2017, and 2018) (B) annual NDVI time series.

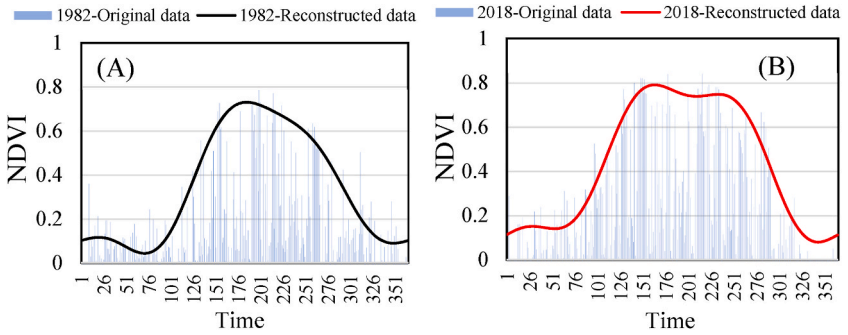

Fig. 4. Results of curve fitting on one pixel in 1982 (A) and 2018 (B).

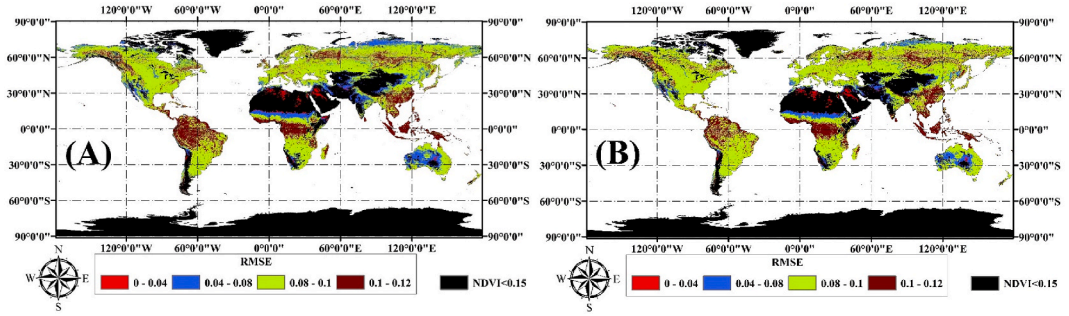

Fig. 5. Spatial distribution of the RMSE means of NDVI for the four historic annual time series (A), and four recent annual time series (B).

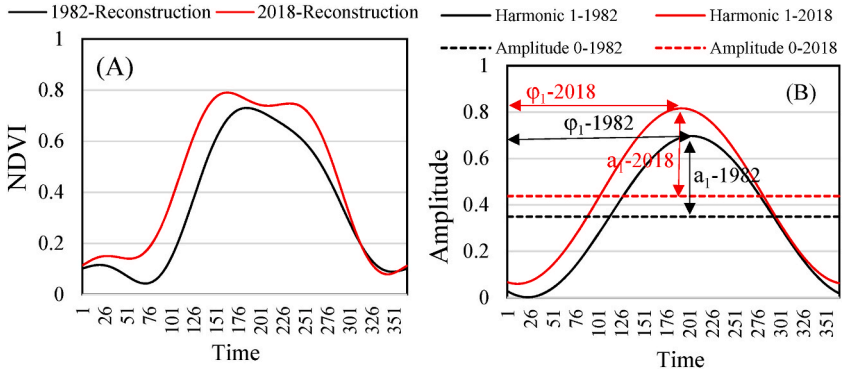

Fig. 6. Reconstruction results of annual NDVI signal for one pixel in 1982 and 2018 (A) and the associated harmonic components (mean and annual) of each signal in 1982 and 2018 (B).

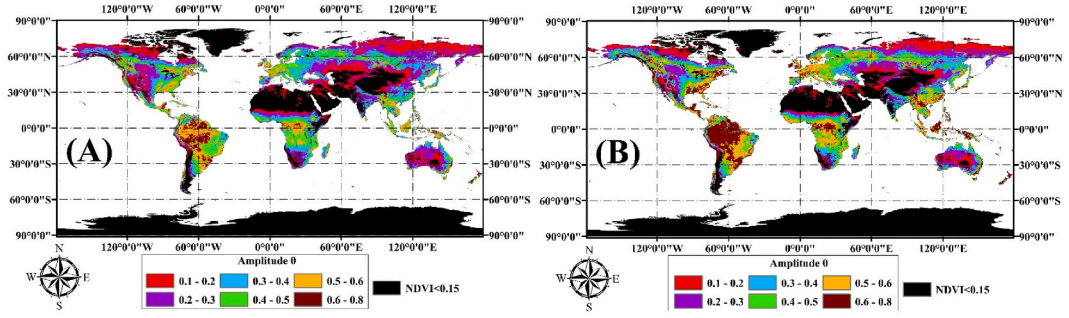

Fig. 7. Mean amplitude 0 of four historical annual time series (A) and four recent annual time series (B).

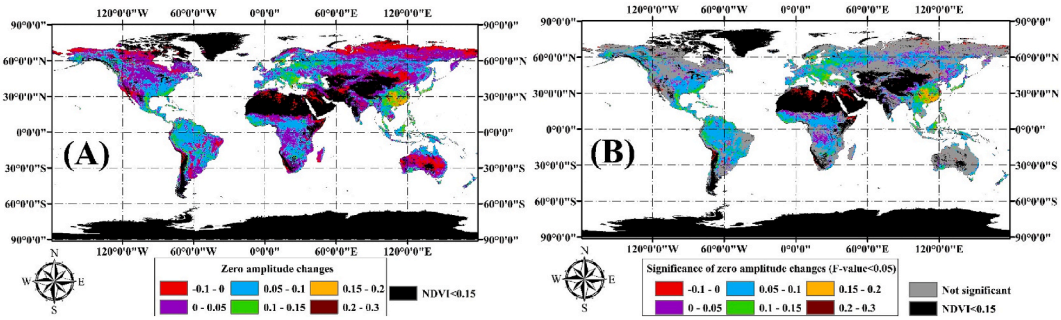

Fig. 8. Mean difference of amplitude 0 between four recent annual NDVI time series and four historical annual NDVI time series (A), and map of significant mean differences (B).

central Australia and regions around the deserts of the globe have a reduced amplitude 0 (deserts and xeric shrubland and tundra biomes). In the other regions around the world, the amplitude 0 is increased. Generally, the average of the NDVI index in the recent time series compared to the past 0.034 has increased.

Regions with significant increases of amplitude 0 (Fig. 8B) over the past three decades (F-value<0.05) are noticed in areas around 60° N, with further expansion over Europe, southeast North America, Amazon forests in South America, Central Africa, and southeast China (confluence of 30° N and 120° E). Changes in other regions were not significant (F-value>0.05).

3.2.2. Annual amplitude of NDVI time series

The means harmonic amplitude 1of four annual time series in both historic and current periods are shown in Fig. 9. Harmonic amplitude 1 indicates the annual amplitude because when the baseline period (365 images) is divided by the harmonic 1, 365 is obtained, which indicates an annual period. Annual harmonic amplitude shows the changes in NDVI over a year. The annual amplitude is low in vegetation-free regions (central Australia) and biomes with evergreen plant species (e.g. tropical and subtropical moist broadleaf forests biome). Moreover, with an increase in vegetation coverage and its changes, the annual harmonic amplitude is increased. Maximum annual amplitude occurs when the amount of greenness in deciduous vegetation coverage is at its maximum level. According to Fig. 9A–B, the annual harmonic amplitude is higher in the deciduous forests of North America, Europe and Asia (e.g. temperate broadleaf and mixed forests biome) than in evergreen vegetation coverage. Further, the annual harmonic amplitude is increased in the vegetation coverage above 60° N. This is due to the elevated amplitude of changes occurring as a result of snow melting and consequent increase in NDVI.

The differences between annual amplitude changes in recent and historic years are shown in Fig. 10A–B, respectively. Although harmonic amplitude 1 is increased in most regions of the world, significant changes (F-value<0.05) were noticed only in a few areas. The maximum increase in harmonic amplitude 1 is seen in areas above 30° N.

3.2.3. Spatial changes in annual phases of NDVI time series

Fig. 11A–B show the mean value of annual phases or harmonic phase 1 for both historic and recent annual time series. The annual phase shows the angular position of the start of the annual signal. Phases in the HANTS algorithm can translate to the start of growing season and plant phenology processes. The mean values of the annual phase of the globe in four historic annual time series and four recent annual time series are 195° and 186°, respectively. Since in HANTS algorithm annual phases are divided into 360° in a trigonometric circle and each year includes 365 days, each degree of phase difference shows a one-day change in the growth and phenological processes. The results show an average of 9° phase difference all over the world between the four historic and recent annual time series. Therefore, annual cycles of vegetation coverage changes occur 9 days earlier on average around the world. The mean annual phase in the northern hemisphere is 212° in the historic time series and 200° in the recent time series, and the mean

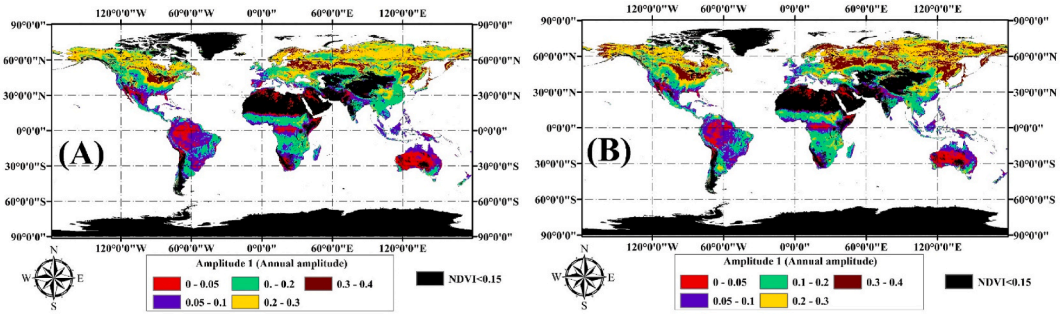

Fig. 9. Mean annual amplitude of four historical annual time series (A) and four recent annual time series (B).

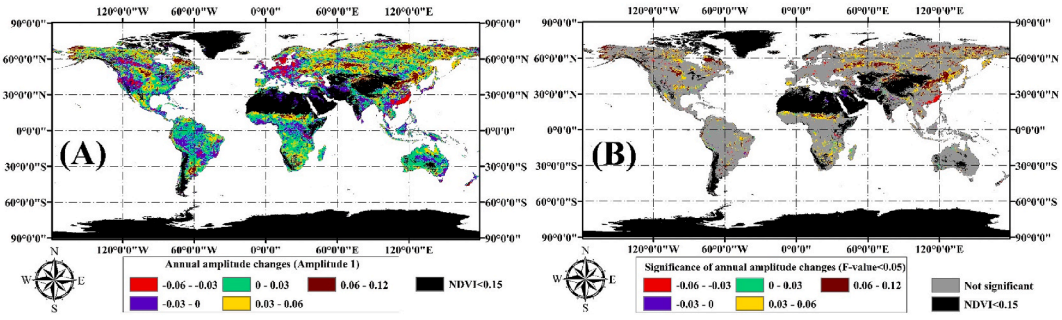

Fig. 10. Mean difference of annual amplitude between both four historic and recent annual NDVI time series (A), and map of significant mean differences (B).

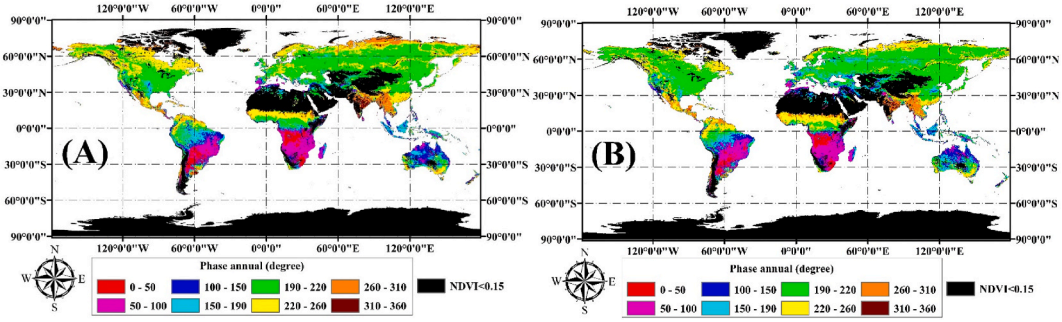

Fig. 11. Mean annual phase of four historical annual time series (A) and four recent annual time series (B).

annual phase in the southern hemisphere is 128.7° in the historic time series and 127.9° in the recent time series. Hence, the maximum annual phase changes have occurred in the northern hemisphere so that the start of growth and plant phenology processes in the northern hemisphere have accelerated by 12° or 12 days compared to the past. Most of these changes can be seen in biomes such as boreal forests (Taiga), temperature broadleaf and mixed forests, temperature conifer forests, temperature grasslands, savannas and shrublands and Mediterranean forests, woodlands and scrub (Fig. 1). On the other hand, annual phase changes in the south hemisphere are minimal. However, mean annual phase changes between both periods are 78° higher in the northern than southern hemisphere. This means that the annual plant cycles start 2–3 months later in the northern hemisphere than in the southern hemisphere.

The mean phase difference map of both time series as well as a significant difference map at 95% probability level are illustrated in Fig. 12A and B. As shown, the maximum annual phase changes are significant in the northern hemisphere at >30° latitude (F-value<0.05).

Fig. 13 demonstrates the mean annual phase changes between both annual NDVI time series along different latitudes (40° S to 80° N) where changes were noticed. As indicated, the mean phase of the recent time series in each latitude of 18–72° N is lower than its corresponding mean phase in the past time series, and its curve is located beneath the historic annual phase curve. As mentioned, reduced phases in recent time series indicate the earlier start of growth and plant phenology processes in these regions. Fig. 13 also shows more intense annual phase changes in the northern hemisphere.

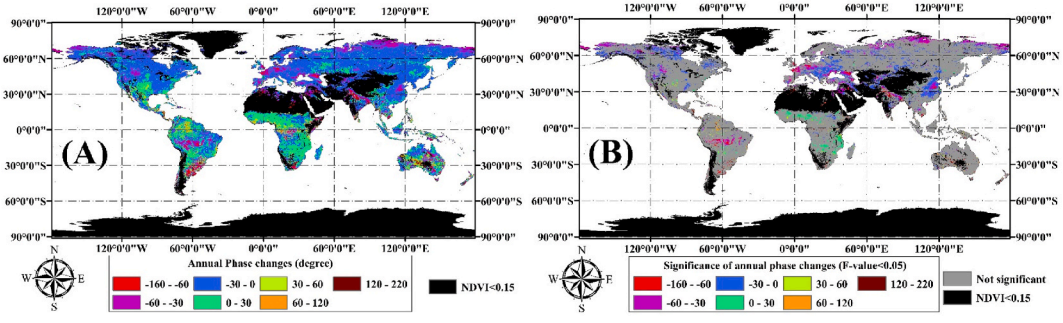

Fig. 12. Mean annual phase difference between both recent and historic annual NDVI time series (A), and the map of significant mean differences (B).

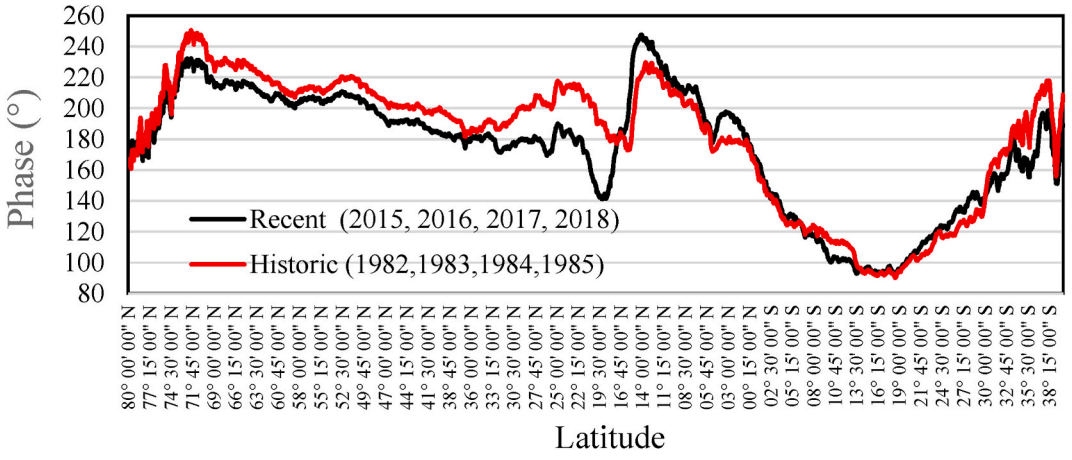

Fig. 13. Mean annual phase changes in both historic and recent periods along latitude 40° S to latitude 80° N.

3.3. Changes in harmonic components in different biomes

Table 2 presents the mean changes of harmonic components in both time series in different global biomes. The amplitude 0 changes were not significant in deserts and xeric shrublands (F-value>0.05), but were significant in tundra, temperate grasslands, savannas, and shrublands (F-value<0.05) and in all the other biomes (F-value<0.01). In general, amplitude 0 and amplitude 1 in most biomes increased significantly from historic to recent time series (Table 2). Increased amplitude 0 indicates an overall increase in vegetation coverage, and increased amplitude 1 can be due to an increase in vegetation coverage in the growth season or higher presence of vegetation (e.g. deciduous trees or plants) which increase greenness rate in only one season of the year. Furthermore, the elevated amplitude can also be indicative of increased changes in vegetation (imbalance). According to Table 2, the annual phase changes were significant in the temperate regions between latitudes 30° and 60° as well as high latitudes (>60°). In all these regions, annual phases significantly reduced, indicating that growth signals in these regions start earlier than before.

Annual phases in boreal forests/taiga; Mediterranean forests, woodlands, and scrubs; temperate broadleaf and mixed forests; temperate grasslands, savannas and shrublands; and deserts and xeric shrublands significantly reduced by 14.1, 14.8, 10.6, 9.5, and 22.8 days, respectively, compared to the past. However, annual phase changes of vegetation coverage in tropical and subtropical areas were not significant (F-value>0.05).

4. Discussion

The results showed that the gaps in remote sensing datasets are lower in the recent than historic time series, especially around 60°N. This decrease is mainly caused by a reduced cloud cover (NaN results, not shown) and related withdrawal of snow and ice cover due to global warming. The North Pole has undergone the largest and quickest amount of warming over the past thirty years [50]. This withdrawal of ice and snow cover has been accelerated by increasing absorption of radiation by the surface [51]. Many studies have documented the reduced snow and ice cover in the northern regions [52–55].

Reduced snow and ice cover and increased solar absorption along high latitudes can justify the elevated NDVI from historic to current periods and reduced annual phases. The results of the current study show that amplitude 0, annual amplitude, and annual phases have undergone significant changes, especially in high altitudes. Amplitude 0 or mean NDVI in most global biomes significantly increased (F-value<0.01). These changes show increased production and seasonal length growth in these regions, especially in the forest biomes along latitudes. This is thought to be a consequence of global warming in the past three decades. For example, amplitude 0, with NDVI of 0.045 has increased (F-value<0.01) in the boreal forests-taiga biome compared to the last three decades. In the taiga biome and regions close to the pole, primary production is limited by temperature [56]. The increased production in these regions has been reported to be due to climatic changes [57,58].

Eastman et al. [11] determined three classes of changes in the 30-year NDVI time series. The first class included regions with increased amplitude 0 or overall vegetation coverage. The second class consisted of regions with elevated annual amplitude. The third class included regions with both elevated amplitude 0 and annual phase. These changes can be indicative of a change in the composition percentage of different growth patterns such as trees, shrubs, grasslands, and herbaceous cover. By analyzing the changing trends of global NDVI, Eastman et al. [11] found that NDVI has increased by 0.46×10^3, on average, per year from 1982 to 2012. Other studies have also shown that NDVI changes are more intense in the northern than southern hemisphere [2] These results justify the elevated amplitude 0, especially in high latitudes in the present study (Fig. 8 and Table 2). In the present study, amplitude 0 in the recent time series compared to the past 0.034 NDVI has increased.

The annual phases significantly reduced in the recent compared to historic time series in the global biomes of boreal forests/taiga; Mediterranean forests, woodlands, and scrubs; temperate broadleaf and mixed forests; temperate grasslands, savannas, and

Table 2
Mean values of Fourier components (amplitudes and phases) for recent and historic time series and associated differences for global biomes.

Biome Name	Period	Amplitude 0	Amplitude 1	Phase 1
Boreal Forests/Taiga	Recent	0.336	0.262	209.15
	Historic	0.290	0.235	223.32
	Difference	*0.045***	*0.027***	*−14.17***
Tundra	Recent	0.060	0.127	229.51
	Historic	0.064	0.113	231.30
	Difference	*−0.004**	*0.014***	*−1.78*^{ns}
Mediterranean Forests, Woodlands and Scrub	Recent	0.307	0.088	153.26
	Historic	0.262	0.070	168.06
	Difference	*0.045***	*0.018***	*−14.80***
Temperate Broadleaf and Mixed Forests	Recent	0.406	0.217	189.43
	Historic	0.339	0.206	200.06
	Difference	*0.067***	*0.011*^{ns}	*−10.63***
Temperate Conifer Forests	Recent	0.404	0.172	216.70
	Historic	0.341	0.160	222.176
	Difference	*0.063***	*0.012***	*−5.472**
Temperate Grasslands, Savannas and Shrublands	Recent	0.261	0.195	194.04
	Historic	0.235	0.169	203.61
	Difference	*0.026**	*0.026***	*−9.56**
Deserts and Xeric Shrublands	Recent	0.137	0.041	152.78
	Historic	0.139	0.034	175.60
	Difference	*−0.002*^{ns}	*0.007***	*−22.82**
Montane Grasslands and Shrublands	Recent	0.178	0.100	188.64
	Historic	0.157	0.082	185.88
	Difference	*0.021***	*0.018**	*2.75*^{ns}
Flooded Grasslands and Savannas	Recent	0.335	0.158	150.16
	Historic	0.288	0.140	151.42
	Difference	*0.047***	*0.018***	*−1.26*^{ns}
Mangroves	Recent	0.244	0.080	169.60
	Historic	0.198	0.075	163.92
	Difference	*0.046***	*0.005**	*5.68*^{ns}
Tropical and Subtropical Dry Broadleaf Forests	Recent	0.438	0.120	185.55
	Historic	0.388	0.103	184.92
	Difference	*0.050***	*0.017***	*0.62*^{ns}
Tropical and Subtropical Grasslands, Savannas and Shrublands	Recent	0.376	0.111	144.99
	Historic	0.329	0.094	142.36
	Difference	*0.046***	*0.016***	*2.62*^{ns}
Tropical and Subtropical Coniferous Forests	Recent	0.486	0.129	244.64
	Historic	0.410	0.107	241.75
	Difference	*0.076***	*0.021**	*2.89*^{ns}
Tropical and Subtropical Moist Broadleaf Forests	Recent	0.556	0.089	186.14
	Historic	0.479	0.086	190.01
	Difference	*0.077***	*0.003*^{ns}	*−3.87*^{ns}

**: significant at 0.01
*: significant at 0.05
ns: not significant

shrublands; and deserts, and xeric shrublands by 14.1, 14.8, 10.6, 9.5, and 22.8 days, respectively (Table 2). Yet, annual phase changes of vegetation coverage in tropical and subtropical areas were not significant. Reduced annual phases indicate earlier growth and plant phenology processes in these regions, as reported in previous studies. These biomes are mostly located in the latitudes above 30° N and below 30° S. The phenological processes are one of the most sensitive biological indicators to investigate the impact of global warming on terrestrial ecosystems [59,60]. Temperature is one of the most important factors in controlling plant phenology processes, especially in humid temperate regions and high latitudes [37,61]. As a result, the reduction of phases (earlier start of growth processes) and increase NDVI (amplitude 0 and 1) in biomes located in high latitudes indicate the effects of climate change and global warming in these areas.

Varlamova and Solovyev [62] reported a positive trend of NDVI in East Siberia over the past three decades. Moreover, based on the analysis of phenological parameters they showed that the Start of Season (SOS) occurred earlier and End of Season (EOS) happened later in the conifer forests and tundra [62]. Based on [40], vegetation coverage in the Loess Plateau, in China, has also increased based on significant NDVI increases from 1991 to 2000 to 2001–2010. Furthermore, this study showed an increase in phonologic SOS from 3.9 to 6.6 days earlier, while EOS occurred 3.6 and 9.6 days later during both periods, in response to global warming. Our study also showed that amplitude 0 increased and the annual phase decreased in this region.

Our study showed the maximum rate of changes in harmonic components of time series, especially in the annual time series, in the northern hemisphere at latitude >30°. Mean annual global phases have reduced 9 days over the past three decades. However [63], reported a mean annual increase in season length all over the world from 0.22 to 0.34 days during 1982–2012. These authors showed that SOS occurred 2.2 ± 0.6 days per decade earlier during 1982–2002 in vegetation types found at moderate (40°) and high (60°)

latitudes in the northern hemisphere, while EOS happened 0.78 ± 0.6 days later. In broadleaf forests the SOS occurred earlier by 2 ± 0.5 days per decade, while EOS occurred later by 2.7 ± 0.6 days from 1982 to 2013 [63]. In the current study, it was also shown that the annual phase in the temperate broadleaf and mixed forests biome has significantly decreased (F-value<0.01) by 10.6 days during three decades.

In general, the findings indicated the high capability of the HANTS algorithm and Fourier series in the analysis of plant phenology changes associated with environmental factors.

5. Conclusions

In the present study, the changes of NDVI harmonic components over the past three decades were investigated using four historical annual time series and four recent annual time series. The main conclusions can be summarized as follows.

1. The number of gaps and errors in remote sensing data series (by cloud, snow and ice cover) at high latitudes (around the 60° N) has decreased from historic to current periods. This decrease is due to the effects of global warming in these areas and associated melting of snow and ice cover.
2. The HANTS algorithm can effectively recover gaps and outliers in NDVI time series. Decomposition of time series into its components can be used effectively to identify changes in vegetation.
3. Most vegetation and biomes on Earth recorded significant changes on mean, annual and seasonal changes on NDVI (amplitude) from 1982 to 1985 to 2015–2018 time series, as well as in plant growth and phenological processes (phases). These changes were more severe in the northern hemisphere than in the southern hemisphere and more pronounced at latitudes above 30°N and below 30°S. These were more noticed on boreal forests/taiga biome time series.
4. Annual changes in vegetation related to the beginning of the growing season and phenological processes showed an average decrease of 9 days from historic to recent NDVI time series. This decrease attained 22.8 days in deserts, and xeric shrublands biomes, 14.8 days in Mediterranean forests, woodlands, and scrubs, 14.1 days in boreal forests/taiga, 10.6 days in temperate broadleaf and mixed forests, and 9.5 days in temperate grasslands, savannas, and shrublands.

Changes in vegetation are thought to be a consequence of global warming, and thus they are expected to continue in the future, with relevant impacts on current spatial distribution of biomes.

Author contribution statement

Hadi Khormizi: Performed the experiments, Analyzed and interpreted the data, Wrote the paper. Hamid Malamiri: Conceived and designed the experiments, Analyzed and interpreted the data, and Wrote the paper. Sahar Alian: Analyzed and interpreted the data, and Wrote the paper. Alfred Stein: Analyzed and interpreted the data, and Wrote the paper. Zahra Kalantari: Analyzed and interpreted the data, and Wrote the paper. Carla Ferreira: Analyzed and interpreted the data, and Wrote the paper.

Data availability statement

Data will be made available on request.

Additional information

Supplementary content related to this article has been publish online at [URL].

Declaration of competing interest

The authors declare that they have no known competing financial interests or personal relationships that could have appeared to influence the work reported in this paper.

References

[1] IPCC, Summary for policymakers. In: climate change 2013: the physical science basis, in: T.F. Stocker, D. Qin, G.-K. Plattner, M. Tignor, S.K. Allen, J. Boschung, A. Nauels, Y. Xia, V. Bex, P.M. Midgley (Eds.), Contribution of Working Group I to the Fifth Assessment Report of the Intergovernmental Panel on Climate Change, Cambridge University Press, Cambridge, United Kingdom and New York, NY, USA, 2013.
[2] Y. Liu, Y. Li, S. Li, S. Motesharrei, Spatial and temporal patterns of global NDVI trends: correlations with climate and human factors, Rem. Sens. 7 (10) (2015) 13233–13250, https://doi.org/10.3390/rs71013233.
[3] D. Zhou, G. Fan, R. Huang, Z. Fang, Y. Liu, H. Li, Interannual variability of the normalized difference vegetation index on the Tibetan Plateau and its relationship with climate change, Adv. Atmos. Sci. 24 (3) (2007) 474–484, https://doi.org/10.1007/s00376-007-0474-2.
[4] J.L. Hatfield, J.H. Prueger, Temperature Extremes: Effect on Plant Growth and Development, vol. 10, Weather and Climate Extremes, 2015, pp. 4–10. Part A.
[5] G. Zhang, X. Xu, C. Zhou, H. Zhang, H. Ouyang, Responses of grassland vegetation to climatic variations on different temporal scales in Hulun Buir Grassland in the past 30 years, J. Geogr. Sci. 21 (4) (2011) 634–650, https://doi.org/10.1007/s11442-011-0869-y.
[6] Y. Xu, J. Yang, Y. Chen, NDVI-based vegetation responses to climate change in an arid area of China, Theor. Appl. Climatol. 126 (1–2) (2016) 213–222, https://doi.org/10.1007/s00704-015-1572-1.

[7] X. Bai, W. Zhao, J. Wang, C.S.S. Ferreira, Precipitation drives the floristic composition and diversity of temperate grasslands in China, Global Ecology and Conservation 32 (2021), e01933, https://doi.org/10.1016/j.gecco.2021.e01933.

[8] A. Chakraborty, P.K. Joshi, A. Ghosh, G. Areendran, Assessing biome boundary shifts under climate change scenarios in India, Ecol. Indicat. 34 (2013) (2013) 536–547.

[9] W. Verhoef, M. Menenti, S. Azzali, Cover A colour composite of NOAA AVHRR- NDVI based on time series analysis (1981-1992), Int. J. Rem. Sens. 17 (2) (1996) 231–235, https://doi.org/10.1080/01431169608949001.

[10] X.W. Chuai, X.J. Huang, W.J. Wang, G. Bao, NDVI, temperature and precipitation changes and their relationships with different vegetation types during 1998–2007 in Inner Mongolia, China, Int. J. Climatol. 33 (7) (2013) 1696–1706, https://doi.org/10.1002/joc.3543.

[11] J.R. Eastman, F. Sangermano, E.A. Machado, J. Rogan, A. Anyamba, Global trends in seasonality of normalized difference vegetation index (NDVI), 1982-2011, Rem. Sens. 5 (10) (2013) 4799–4818, https://doi.org/10.3390/rs5104799.

[12] D. Mao, Z. Wang, L. Luo, C. Ren, Integrating AVHRR and MODIS data to monitor NDVI changes and their relationships with climatic parameters in Northeast China, Int. J. Appl. Earth Obs. Geoinf. 18 (2012) 528–536, https://doi.org/10.1016/j.jag.2011.10.007.

[13] H.R. Ghafarian Malamiri, H. Zare Khormizi, Investigating vegetation changes in Iran using NDVI time series of NOAA-AVHRR sensor and Harmonic ANalysis of Time Series (HANTS), Scient.-Res. Quart. Geograph. Data (SEPEHR) 29 (113) (2020) 141–158, https://doi.org/10.22131/sepehr.2020.40476.

[14] H.R. Ghafarian Malamiri, H. Zare, I. Rousta, H. Olafsson, E. Izquierdo Verdiguier, H. Zhang, T.D. Mushore, Comparison of harmonic analysis of time series (HANTS) and multi-singular spectrum analysis (M-SSA) in reconstruction of long-gap missing data in NDVI time series, Rem. Sens. 12 (17) (2020) 2747, https://doi.org/10.3390/rs12172747.

[15] I. Garonna, R. De Jong, M.E. Schaepman, Variability and evolution of global land surface phenology over the past three decades (1982–2012), Global Change Biol. 22 (4) (2016) 1456–1468, https://doi.org/10.1111/gcb.13168.

[16] H. Zare khormizi, S.Z. Hosseini, M.H. mokhtari, H.R. Ghafarian Malamiri, Reconstruction of MODIS NDVI time series using harmonic analysis of time series algorithm (HANTS), J. Spatial Plan. 21 (3) (2017) 221–255.

[17] Z. Xue, P. Du, L. Feng, Phenology-driven land cover classification and trend analysis based on long-term remote sensing image series, IEEE J. Sel. Top. Appl. Earth Obs. Rem. Sens. 7 (4) (2014) 1142–1156, https://doi.org/10.1109/JSTARS.2013.2294956.

[18] H. Zare khormizi, H. Ghafarian Malamiri, Effect of height and temperature on plant phenological processes using harmonic analysis of MODIS NDVI time series (Case study: shirkouh, Yazd province), Iranian J. Remote Sensing & GIS 12 (3) (2020) 1–22, https://doi.org/10.52547/ijrsgis.2021.213651.0.

[19] H.R. Ghafarian Malamiri, I. Rousta, H. Olafsson, H. Zare, H. Zhang, Gap-filling of MODIS time series land surface temperature (LST) products using singular spectrum analysis (SSA), Atmosphere 9 (9) (2018) 334, https://doi.org/10.3390/atmos9090334.

[20] C. Wu, X. Hou, D. Peng, A. Gonsamo, S. Xu, Land surface phenology of China's temperate ecosystems over 1999-2013: spatial–temporal patterns, interaction effects, covariation with climate and implications for productivity, Agric. For. Meteorol. 216 (2016) 177–187, https://doi.org/10.1016/j.agrformet.2015.10.015.

[21] W. Verhoef, Application of harmonic analysis of NDVI time series (HANTS), in: S. Azzali, M. Menenti (Eds.), Fourier Analysis of Temporal NDVI in Southern Africa and America Continent. The Netherlands, vol. 108, DLO Winand Staring Centre, Report, 1996, pp. 19–24.

[22] M.E. Jakubauskas, D.R. Legates, J.H. Kastens, Crop identification using harmonic analysis of time-series AVHRR NDVI data, Comput. Electron. Agric. 37 (2002) 127–139, https://doi.org/10.1016/S0168-1699(02)00116-3.

[23] G.J. Roerink, M. Menenti, W. Verhoef, Reconstructing cloudfree NDVI composites using Fourier analysis of time series, Int. J. Rem. Sens. 21 (9) (2000) 1911–1917, https://doi.org/10.1080/014311600209814.

[24] L. Zhou, Y. Tian, R.B. Myneni, P. Ciais, S. Saatchi, Y.Y. Liu, T. Hwang, Widespread decline of Congo rainforest greenness in the past decade, Nature 509 (7498) (2014) 86, https://doi.org/10.1038/nature13265.

[25] H. Ghafarian Malamiri, H. Zare Khormizi, Reconstruction of cloud-free time series satellite observations of land surface temperature (LST) using harmonic analysis of time series algorithm (HANTS), J. RS and GIS for Nat. Res. 8 (3) (2017) 37–55.

[26] Y. Julien, J.A. Sobrino, Comparison of cloud-reconstruction methods for time series of composite NDVI data, Rem. Sens. Environ. 114 (3) (2010) 618–625, https://doi.org/10.1016/j.rse.2009.11.001.

[27] Y. Xu, Y. Shen, Reconstruction of the land surface temperature time series using harmonic analysis, Comput. Geosci. 61 (2013) 126–132, https://doi.org/10.1016/j.cageo.2013.08.009.

[28] J. Zhou, L. Jia, M. Menenti, Reconstruction of global MODIS NDVI time series: performance of harmonic analysis of time series (HANTS), Rem. Sens. Environ. 163 (15) (2015) 217–228, https://doi.org/10.1016/j.rse.2015.03.018.

[29] J. Wen, Z. Su, Y.M. Ma, Reconstruction of a cloud-free vegetation index time series for the Tibetan Plateau, Mt. Res. Dev. 24 (4) (2004) 348–353, https://doi.org/10.1659/0276-4741(2004)024[0348:ROACVI]2.0.CO;2.

[30] P. Lesica, P.M. Kittelson, Precipitation and temperature are associated with advanced flowering phenology in semi-arid grassland, J. Arid Environ. 74 (2010) 1013–1017, https://doi.org/10.1016/j.jaridenv.2010.02.002.

[31] M.A. White, K.M. de Beurs, K. Didan, D.W. Inouye, A.D. Richardson, O.P. Jensen, J.F. Brown, Intercomparison, interpretation, and assessment of spring phenology in North America estimated from remote sensing for 1982-2006, Global Change Biol. 15 (10) (2009) 2335–2359, https://doi.org/10.1111/j.1365-2486.2009.01910.x.

[32] A.D. Richardson, T.F. Keenan, M. Migliavacca, Y. Ryu, O. Sonnentag, M. Toomey, Climate change, phenology, and phenological control of vegetation feedbacks to the climate system, Agric. For. Meteorol. 169 (2013) 156–173, https://doi.org/10.1016/j.agrformet.2012.09.012.

[33] M.P. Dannenberg, C. Song, T. Hwang, E.K. Wise, Empirical evidence of El Niño–Southern Oscillation influence on land surface phenology and productivity in the western United States, Rem. Sens. Environ. 159 (2015) 167–180, https://doi.org/10.1016/j.tree.2020.01.010.

[34] Q. Liu, Y.H. Fu, Z. Zhu, Y. Liu, Z. Liu, M. Huang, S. Piao, Delayed autumn phenology in the Northern Hemisphere is related to change in both climate and spring phenology, Global Change Biol. 22 (11) (2016) 3702–3711, https://doi.org/10.1111/gcb.13311.

[35] R.I. Bertin, Plant phenology and distribution in relation to recent climate change, J. Torrey Bot. Soc. 135 (1) (2008) 126–146, https://doi.org/10.1016/j.agrformet.2019.107803.

[36] H. Yu, E. Luedeling, J. Xu, Winter and spring warming result in delayed spring phenology on the Tibetan Plateau, Proc. Natl. Acad. Sci. USA 107 (51) (2010) 22151–22156, https://doi.org/10.1073/pnas.1012490107.

[37] M. Pellerin, A. Delestrade, G. Mathieu, O. Rigault, N.G. Yoccoz, Spring tree phenology in the Alps: effects of air temperature, altitude and local topography, Eur. J. For. Res. 131 (6) (2012) 1957–1965, https://doi.org/10.1007/s10342-012-0646-1.

[38] S. Piao, P. Friedlingstein, P. Ciais, N. Viovy, J. Demarty, Growing season extension and its impact on terrestrial carbon cycle in the Northern Hemisphere over the past 2 decades, Global Biogeochem. Cycles 21 (3) (2007), https://doi.org/10.1029/2006GB002888.

[39] C. Atzberger, P.H. Eilers, A time series for monitoring vegetation activity and phenology at 10-daily time steps covering large parts of South America, Int. J. Digital Earth 4 (5) (2011) 365–386, https://doi.org/10.1080/17538947.2010.505664.

[40] E. Yan, G. Wang, H. Lin, C. Xia, H. Sun, Phenology-based classification of vegetation cover types in Northeast China using MODIS NDVI and EVI time series, Int. J. Rem. Sens. 36 (2) (2015) 489–512, https://doi.org/10.1080/01431161.2014.999167.

[41] M. Jakubauskas, D.R. Legates, Harmonic analysis of time-series AVHRR NDVI data for characterizing US Great Plains land use/land cover, Int. Archiv. Photogram. Remote Sensing 33 (B4/1; PART 4) (2000) 384–389.

[42] N.A. Campbell, Biology, fourth ed., The Benjamin/Cummings Publishing Company, Inc., Menlo Park, California, 1996 via UC Berkeley, The World's Biomes, Available: http://www.ucmp.berkeley.edu/glossary/gloss5/biome/.

[43] D.M. Olson, E. Dinerstein, E.D. Wikramanayake, N.D. Burgess, G.V.N. Powell, E.C. Underwood, K.R. Kassem, Terrestrial ecoregions of the world: a new map of life on Earth, Bioscience 51 (11) (2001) 933–938.

[44] J.W. Rouse, R.H. Haas, J.A. Schell, D.W. Deering, Monitoring vegetation systems in the great plains with ERTS, 3rd ERTS Symposium, NASA SP- 351 I (1973) 309–317.

[45] E. Vermote, C. Justice, I. Csiszar, J. Eidenshink, R. Myneni, F. Masuoka Baret, Robert Wolfe, Claverie Martin, NOAA CDR Program, NOAA climate data Record (CDR) of normalized difference vegetation index (NDVI), Version 4 [1982–2014], NOAA National Climatic Data Center, 2014, https://doi.org/10.7289/V5PZ56R6.
[46] M. Menenti, S. Azzali, W. Verhoef, R. Van Swol, Mapping agroecological zones and time lag in vegetation growth by means of Fourier analysis of time series of NDVI images, Adv. Space Res. 13 (5) (1993) 233–237, https://doi.org/10.1016/0273-1177(93)90550-U.
[47] J. Fourier, Note relative aux vibrations des surfaces élastiques et au mouvement des ondes, Bulletin des Sciences par Société Philomatique 1 (1818) 126–136.
[48] J. Wu, L.P. Albert, A.P. Lopes, N. Restrepo-Coupe, M. Hayek, K.T. Wiedemann, J.V. Tavares, Leaf development and demography explain photosynthetic seasonality in Amazon evergreen forests, Science 351 (6276) (2016) 972–976, https://doi.org/10.1126/science.aad5068.
[49] H. Zare Khormizi, H. Ghafarian Malamiri, Investigation of phenological components changes of Iranian vegetation in response to climate change using NDVI products of AVHRR sensor from 1982 to 2018, J. RS and GIS for Nat. Res. 11 (4) (2020) 87–113, dorl.net/dor/20.1001.1.26767082.1399.11.4.5.5.
[50] K.E. Trenberth, P.D. Jones, P. Ambenje, R. Bojariu, D. Easterling, A. Klein Tank, B. Soden, Observations: surface and atmospheric climate change, Clim. Change (2007) 235–336 (Chapter 3).
[51] R.G. Graversen, T. Mauritsen, M. Tjernstrom, E. Kallen, G. Svensson, Vertical structure of recent Arctic warming, Nature 451 (7174) (2008) 53, https://doi.org/10.1038/nature06502.
[52] O.N. Bulygina, P.Y. Groisman, V.N. Razuvaev, N.N. Korshunova, Changes in snow cover characteristics over Northern Eurasia since 1966, Environ. Res. Lett. 6 (4) (2011), 045204, https://doi.org/10.1088/1748-9326/6/4/045204.
[53] R. Brown, C. Derksen, L. Wang, A multi-data set analysis of variability and change in Arctic spring snow cover extent, 1967–2008, J. Geophys. Res. Atmos. 115 (D16) (2010), https://doi.org/10.1126/sciadv.aax3308.
[54] R.D. Brown, Northern Hemisphere snow cover variability and change, 1915-97, J. Clim. 13 (13) (2000) 2339–2355, https://doi.org/10.1002/wea.3625.
[55] E.S. Euskirchen, A.D. McGuire, F.S. Chapin III, Energy feedbacks of northern high-latitude ecosystems to the climate system due to reduced snow cover during 20th century warming, Global Change Biol. 13 (11) (2007) 2425–2438, https://doi.org/10.1111/j.1365-2486.2007.01450.x.
[56] J. Schultz, The Ecozones of the World: the Ecological Divisions of the Geosphere, second ed., Springer, New York, NY, USA, 2005.
[57] K.C. Guay, P.S. Beck, L.T. Berner, S.J. Goetz, A. Baccini, W. Buermann, Vegetation productivity patterns at high northern latitudes: a multi-sensor satellite data assessment, Global Change Biol. 20 (10) (2014) 3147–3158, https://doi.org/10.1111/gcb.12647.
[58] R.B. Myneni, C.D. Keeling, C.J. Tucker, G. Asrar, R.R. Nemani, Increased plant growth in the northern high latitudes from 1981 to 1991, Nature 386 (6626) (1997) 698, https://doi.org/10.1038/386698a0.
[59] M. Shen, Y. Tang, J. Chen, X. Zhu, Y. Zheng, Influences of temperature and precipitation before the growing season on spring phenology in grasslands of the central and eastern Qinghai-Tibetan Plateau, Agric. For. Meteorol. 151 (12) (2011) 1711–1722, https://doi.org/10.1016/j.agrformet.2011.07.003.
[60] Z. Zheng, W. Zhu, G. Chen, N. Jiang, D. Fan, D. Zhang, Continuous but diverse advancement of spring-summer phenology in response to climate warming across the Qinghai-Tibetan Plateau, Agric. For. Meteorol. 223 (2016) 194–202, https://doi.org/10.1016/j.agrformet.2016.04.012.
[61] T.G. Workie, H.J. Debella, Climate change and its effects on vegetation phenology across ecoregions of Ethiopia, Global Ecol. Conserv. 13 (2017), e00366, https://doi.org/10.1016/j.gecco.2017.e00366.
[62] E. Varlamova, V. Solovyev, Study of NDVI vegetation index in East Siberia under global warming, in: 22nd International Symposium on Atmospheric and Ocean Optics: Atmospheric Physics, vol. 10035, International Society for Optics and Photonics, 2016, p. 100355K, https://doi.org/10.1117/12.2248092.
[63] J. Zhao, H. Zhang, Z. Zhang, X. Guo, X. Li, C. Chen, Spatial and temporal changes in vegetation phenology at middle and high latitudes of the Northern Hemisphere over the past three decades, Rem. Sens. 7 (8) (2015) 10973–10995, https://doi.org/10.3390/rs70810973.